Desalination and Water Treatment
www.deswater.com
doi: 10.5004/dwt.2023.29605

296 (2023) 83–91
June

Degradation of Rhodamine B by persulfate activation with iron-loaded biochar

Yang Yang[a],·Hongyang Lin[a],·Shuhui Wu[a],·Xue Yao[a],·Xuedong Feng[b], Yanfei Ma[b,*]

[a]*School of Agricultural Engineering and Food Science, Shandong University of Technology, Zibo 255000, China, emails: 21403010279@stumail.edu.cn (Y. Yang), 577697469@qq.com (H.Y. Lin), 2444538563@qq.com (S.H. Wu), Yaoxue199901@163.com (X. Yao)*
[b]*School of Resource and Environmental Engineering, Shandong University of Technology, Zibo 255000, China, emails: mayanfei@sdut.edu.cn (Y.F. Ma), rudy1121@163.com (X.D. Feng)*

Received 15 November 2022; Accepted 27 April 2023

ABSTRACT

Conventional wastewater treatment is inefficient in removing Rhodamine B (RhB) from dying wastewater. Wastewater treatment is a promising advanced oxidation process (AOP) based on biochar and iron-activated persulfate. Therefore, the current study explored the potential of iron-loaded biochar-activated persulfate to remove RhB. Based on morphology observation, iron-loaded biochar could be successfully prepared using slow pyrolysis inside an N_2 environment at 800°C. Structure analysis revealed that the surface area of iron-loaded biochar was 1.5 times the size of unmodified biochar. Under the optimum reaction condition, the maximum removal rate of RhB was 99.96%, determined by single-factor experiments. The RhB removal rate was improved with increased activator dosage, PS dosage, and temperature but decreased with increased pH and initial dye concentration. The RhB adsorption rate was governed by pseudo-first-order reaction kinetics, and the Langmuir–Hinshelwood kinetic model (R^2 = 0.99853) helped explain the adsorption behavior. Recycling experiments of Fe-BC indicated a twice-cycle capacity which could be improved. Free radical quenching experiments showed that sulfate-free ($SO_4^{\bullet-}$) and hydroxyl ($^{\bullet}OH$) radicals worked together in the RhB removal process, dominated by $^{\bullet}OH$.

Keywords: Persulfate activation; Iron loaded biochar; Advanced oxidation Process; Rhodamine B; Kinetics

1. Introduction

In the past few decades, many technologies have been incorporated for dying wastewater treatment, such as physical adsorption, biological methods, and chemical oxidation [1]. Advanced oxidation processes (AOPs), such as Fenton oxidation, electrochemical oxidation, ozonation, and photooxidation, have attracted widespread attention due to environmental friendliness and high efficiency [2,3]. Sulfate-free radicals obtained from persulfate differ from conventional hydroxyl radicals among AOPs. They are becoming a research hotspot due to their broad range of pH value, long-half life, and high selectivity towards degrading organic pollutants [3].

With the rapid industrial development in China, the dye industry is also expanding in scale. Rhodamine B (RhB) represents azo dyes for their good stabilizing ability and dyeing properties. Simultaneously, RhB is prone to mutagenicity, teratogenicity, and carcinogenicity. Moreover, the RhB in wastewater requires economical and efficient removal treatment methods [4].

The persulfate activation is required to increase the removal rate of RhB. The primary activation methods are homogeneous and heterogeneous catalytic activation [4].

* Corresponding author.

Homogeneous activation mainly involves activation systems of energy (including light and electricity) [5,6] and homogeneous metal ions [7]. Heterogeneous activation includes catalysts of heterogeneous metals (such as iron-based, copper-based, etc.) [5] and non-metallic carbons [8]. However, the homogeneous activated catalysts are difficult to separate, recover and regenerate, causing secondary environmental contamination. Thus, researchers investigate the heterogeneous activation catalysts to replace the homogeneous ones [9]. Biochar has a well-developed pore structure, good thermal stability, and abundant functional groups. Biochar can enhance the catalytic activity of persulfate, causing a significant degradation capability and low energy consumption. They have a wide range of application prospects in advanced wastewater oxidation treatment [10–12]. Therefore, biochar is a suitable loaded catalyst carrier to improve its sorption ability through surface modification. Jiang et al. [13] prepared a Fe-functionalized biochar composite with Fe^0 to remove bisphenol A(BPA) by activating peroxymonosulfate. The results indicated that nanofibers (Fe-BC-700°C) enhanced the biochar functional groups. Thus, more active sites were exposed to the reaction, and BPA (20 mg/L) could be removed entirely in 5 min. Fu et al. [14] investigated the peroxymonosulfate activation by novel Fe_3O_4-loaded porous biochar for treating p-hydroxybenzoic acid (HBA). The characterization analysis revealed countless micropores on the surface carbon layer. HBA was entirely removed by the catalyst made at 700°C for 15 min. Shao et al. [15] and Hao et al. [17] demonstrated that iron-loaded biochar could effectively activate persulfate and remove organic pollutants such as tetracycline and Orange G in water. Lyu et al. [16] synthesized engineered biochar from ball-milled sugarcane bagasse biomass at 450°C, showing enhanced methylene blue removal ability. Thus, loading metal oxides on the surface of biochar can significantly regulate its surface properties and increase the catalytic activity for synergistic dying wastewater treatment [16,17].

Peanut shells are extensively available and inexpensive as a common agricultural by-product and can be theoretically loaded with iron oxides to prepare heterogeneous catalysts. Previous studies have revealed that loaded peanut shell catalysts effectively remove the dye. An et al. demonstrated that peroxydisulfate could be efficiently activated by biochar prepared at 700°C. The removal rate of acid Orange 7 could become 96% in 10 min. Xu et al. synthesized peanut shell biochar for activating persulfate and promoting diatrizoate removal. The diatrizoate removal rate reached nearly 100% under optimal conditions. Ikhlaq et al. investigated safranin decolorization using Iron-impregnated peanut shell ash in a UV-assisted heterogeneous Fenton process. Under optimal conditions, the maximum safranin decolorization was 74.76% in the Fe-PSA/H_2O_2/UV process [18–20]. Hence, peanut shells were utilized as biomass in this study to prepare biochar, and the iron-loaded biochar activated persulfate as a catalyst to remove RhB. After use, the unmodified, modified, and biochar properties were characterized to analyze the catalytic effect of iron-loaded on RhB degradation by persulfate. A theoretical basis of waste biomass utilization, persulfate catalyst preparation, and practical applications was provided by investigating the reaction factors and mechanisms influencing persulfate activation for removing RhB by iron-loaded biochar.

2. Experimental set-up

2.1. Chemicals and reagents

We purchased analytically pure Rhodamine B ($C_{28}H_{31}ClN_2O_3$), sodium persulfate ($Na_2S_2O_8$), ferrous sulfate heptahydrate ($FeSO_4{\cdot}7H_2O$), sulfuric acid (H_2SO_4), sodium nitrate ($NaNO_3$), sodium hydroxide (NaOH), methanol (CH_4O), tert-butanol ($C_4H_{10}O$), and anhydrous ethanol (C_2H_6O) from Sinopharm Chemical Reagent Co. Peanut shells were harvested from a Shandong farm. An ultrapure water machine deionized the experimental water.

2.2. Biochar preparation

The appropriate peanut shell (200 g) amounts were selected, repeatedly rinsed using deionized water to neutralize, and dried to constant weight. Biochar was produced by placing peanut shells in a planetary ball mill machine. The milling media was balls, and the milling time was 8 h with a rotation direction change every 2 h at 220 rpm. The media was sieved through 60-mesh into the size fraction: <0.25 mm, and the peanut shell powder was obtained under the mesh for reserve. The peanut shell powder was mixed into 200 mL of $FeSO_4$ (0.014 mol/L) solution. Then 80 mL NaOH (0.09 mol/L) and 120 mL $NaNO_3$ (0.02 mol/L) solutions were added, and the sample was shaken in a thermostatically controlled water bath for 12 h at 90°C. Finally, the treated peanut shell powder was obtained by solid–liquid separation and used to prepare biochar. The modified iron-loaded biochar (Fe-BC) was prepared under nitrogen atmosphere protection in a tube furnace at a heating rate of 5°C/min to 800°C and maintained for 0.5 h. The preparation process of the unmodified peanut shell biochar was the same and was recorded as BC. The resultant Fe-BC and BC were washed several times using deionized water to remove ash, oven-dried at 80°C, and stored in vials before use.

2.3. Characterization of materials and analytical methods

After the reaction, the microscopic morphologies and functional groups of BC, Fe-BC, and Fe-BC were observed using the Quanta 250 environmental Scanning electron microscope (SEM) and Fourier-transform infrared spectrometer (FTIR). The results provided a basis for analyzing the experimental results and discussing the action mechanism. The BC and Fe-BC surface area was taken by N_2 adsorption–desorption with the Brunauer–Emmett–Teller (BET) method.

The RhB concentration in wastewater was analyzed using the UV/vis spectrophotometer, having an absorption wavelength of 554 nm. The RhB removal rate was determined as Eq. (1) follows:

$$\mathrm{Re} = \frac{C_0 - C_t}{C_0} \times 100\% \tag{1}$$

where Re represents the removal rate of RhB, C_0 is the initial RhB concentration, and C_t is the RhB concentration at the time of t.

2.4. Experimental procedure

2.4.1. Verification of the catalytic activity of Fe-BC

The 200 mL solution with RhB (50 mg/L, pH of 4.7) was placed in a 500 mL conical flask. First, the oxidant PS was added into the flask, and then the activator. The mixed sample was shaken at 150 rpm in a constant temperature oscillator for 60 min and 25°C. The samples were obtained from the flask every 10 min.

The experimental system effects with different combinations of activators and oxidants on the removal rate of RhB were designed and represented in Table 1.

2.4.2. Investigation of the factors influencing the RhB removal

The effect of the Fe-BC dosage, PS dosage, pH, initial dye concentration, and temperature on the RhB removal rate was assessed. Four different Fe-BC dosages (0.05, 0.1, 0.2, and 0.3 g/L), PS dosages (1, 2, 3, and 4 mM), temperature (25°C, 30°C, 35°C and 40°C), RhB concentrations (10, 20, 30, and 50 mg/L) and five different pH (3, 4.7, 7, 9 and 11) became the experimental parameters.

Methanol (MA) and tert-Butanol (TBA) were used as free radical quenchers for radical quenching experiments under optimal conditions to identify the main reactive radical species and the catalytic mechanism behind Fe-BC. The added alcohols to PS molar ratio was 200:1 for quenching all the radicals.

Table 1
Experimental systems of different combinations of activators and oxidants

System	Activator type	Activator dosage	Oxidant type	Oxidant dosage
BC	BC	0.05 g/L	/	/
Fe-BC	Fe-BC	0.05 g/L	/	/
PS	/	/	PS	1 mM
BC/PS	BC	0.05 g/L	PS	1 mM
Fe^{2+}/PS	Fe^{2+}	0.035 mM	PS	1 mM
Fe-BC/PS	Fe-BC	0.05 g/L	PS	1 mM

3. Results and discussion

3.1. Characterization of Fe-BC

As shown in Fig. 1c, BC was flaky with a smooth surface and no attached particles. Fig. 1d reveals that the Fe-BC surface was destroyed and irregular, with some regular cubes and columns appearing. Fig. 1a columns are the iron-containing compounds, and most iron aggregated in the regular cubes. Energy spectrum in Fig. 1b indicates that the mass percentage of Fe, O, and C were 69%, 18%, and 12%, respectively. The N_2 adsorption–desorption isotherms and the pore size distribution of BC and Fe-BC are represented in Fig. 2. The N_2 BET surface area of Fe-BC (344.61 m^2/g) was higher than BC (228.01 m^2/g). The specific surface showed a significant increase of 1.5 times BC after loading iron on the surface. Thus, Fe-BC had more pore structure, consistent with the SEM results. The larger specific surface area of Fe-BC was beneficial for pollutant absorption or enrichment and provided more catalytic sites to degrade RhB [21]. The average pore size of Fe-BC and BC were 2.13 nm and 2.35 nm, respectively. The adsorption isotherms of Fe-BC revealed I isotherms (IUPCA classification), which were mainly monolayer adsorption. The adsorption isotherms of BC were type II isotherms, mainly multilayer adsorption

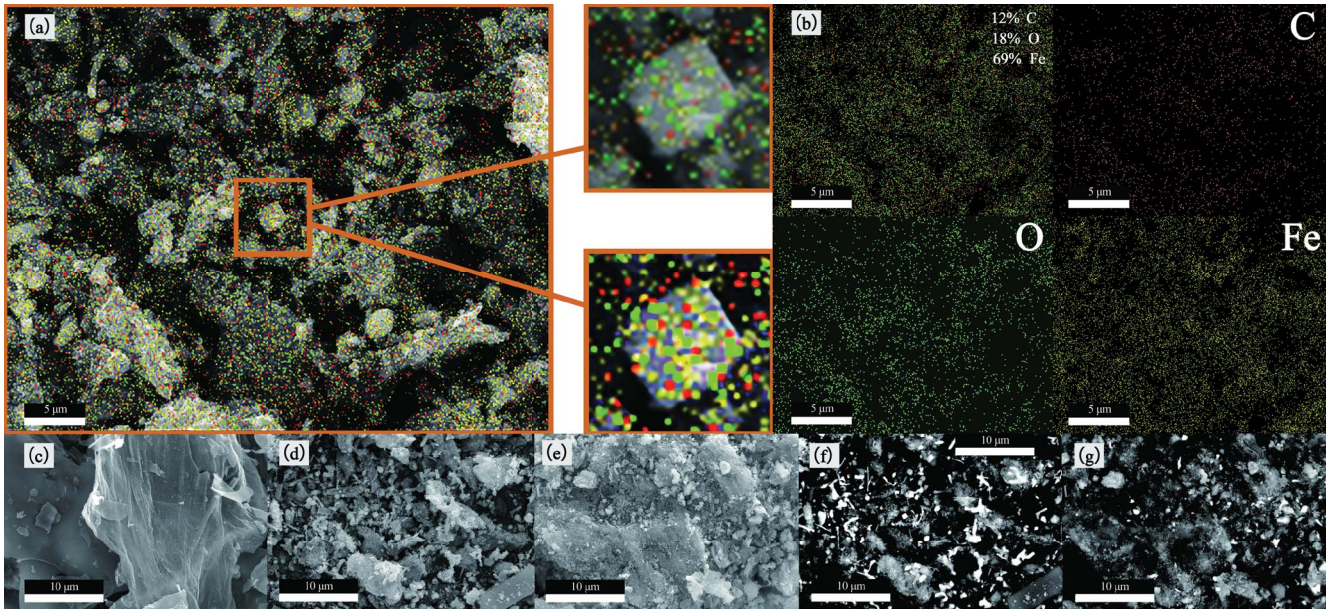

Fig. 1. Characterization of BC and Fe-BC and Fe-BC after reaction EDS mapping of Fe-BC (a) and element distribution of Fe–C–O, (b) SEM micrographs of BC, (c) Fe-BC, (d) and Fe-BC after reaction, (e) EDS images of (back scattered electron) Fe-BC, (f) and Fe-BC after reaction (g).

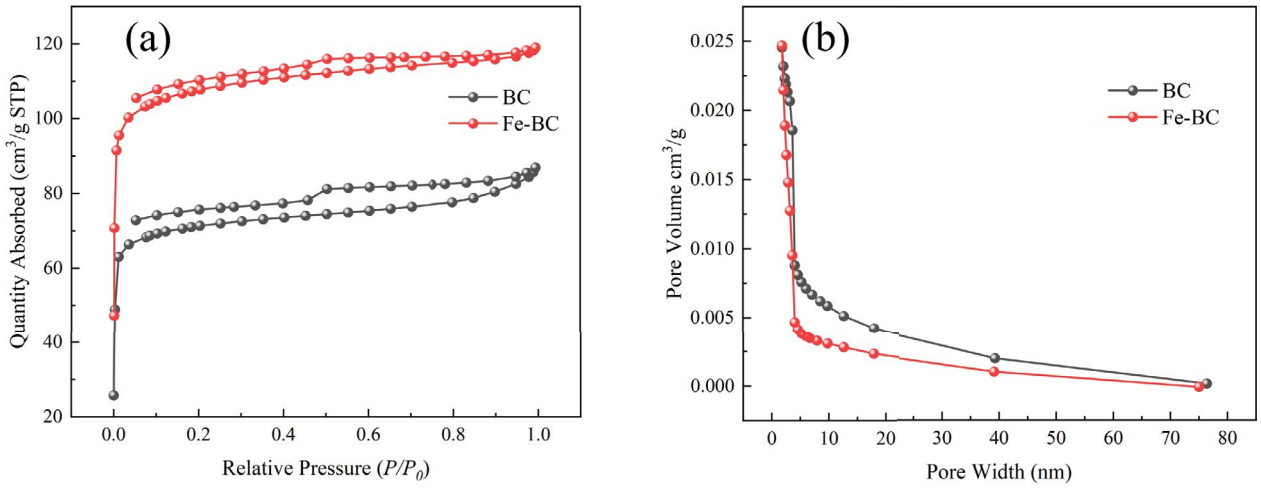

Fig. 2. N_2 adsorption–desorption isotherms (a) and pore size distribution curves of BC and Fe-BC (b).

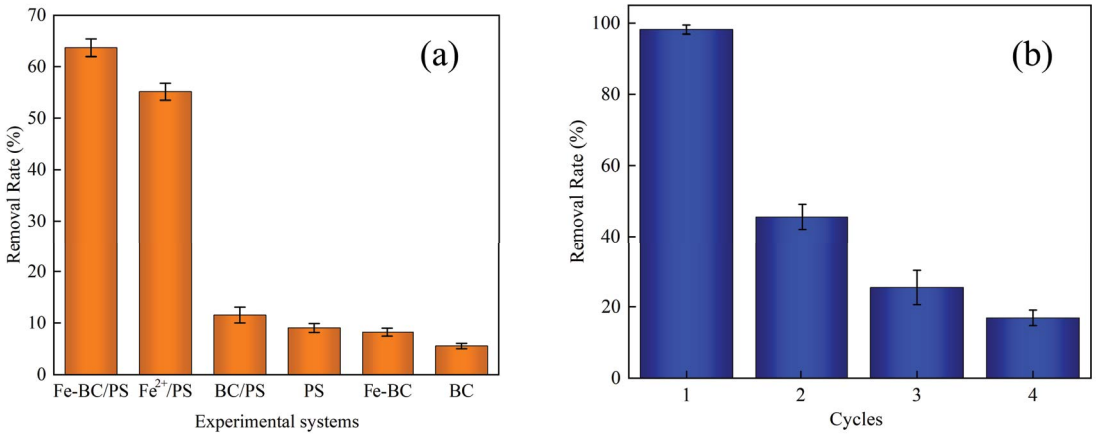

Fig. 3. Effect of different experiment systems on RhB removal and test of recycling of Fe-BC on RhB removal (BC, BC/PS, Fe-BC dosage of 0.05 g/L, Fe^{2+} concentration of 0.035 mM, PS concentration of 1 mM, RhB concentration of 50 mg/L, temperature of 25°C, pH = 4.7).

[22]. Iron-loaded biochar enhanced the specific surface area and pore structure, promoting RhB degradation. Thus, iron elements are uniformly distributed in the regular-shaped cubes, with the successful modification of biochar.

3.2. Evaluation of Fe-BC performance

From Fig. 3a it can be seen that BC, Fe-BC, PS, and BC/PS had a low RhB removal rate of 5.5%, 8.23%, 9.0%, and 11.5% after 60 min of reaction, respectively. Compared to Fe^{2+}/PS and Fe-BC/PS systems, the lower RhB removal rate could be due to three reasons: (i) low absorption capacity of BC and Fe-BC. (ii) although PS had a high redox potential and could oxidize RhB directly, RhB removal efficiency was limited due to the lack of an activator; and iii) persistent radical disappearance on the BC surface at high temperature (800°C) led to the inability to activate PS effectively in the BC/PS system [23]. While PS was activated by adding a concentration of Fe^{2+} (0.035 mM), the removal rate was 55.14% after 60 min of reaction, lower than the Fe-BC/PS system (63.67% after 60 min). Our results were consistent with the findings of Liang et al. Fe^{2+} showed an excellent capacity for activating PS to remove pollutants. However, Fe^{2+} was easily oxidized to Fe^{3+} in an aerobic environment, leading to a low utilization efficiency [24]. The stable iron-loaded biochar could slowly release Fe^{2+}, improving its utilization efficiency and the activating PS effect on RhB removal. Therefore, the Fe-BC/PS system was characterized as the optimal experimental system.

3.3. Study of factors affecting RhB removal in wastewater

3.3.1. Effect of Fe-BC dosage on RhB removal

The RhB removal rate increased from 0.01348 mg/(L·min) (R^2 = 0.97389) to 0.0662 mg/(L·min) (R^2 = 0.90904) since the Fe-BC dosage was increased from 0.05 to 0.3 g/L in Fig. 4a. The larger the Fe-BC dosing, the larger the Fe^{2+} could be released, leading to faster PS activation. However, the catalytic effect did not demonstrate a pronounced increase as

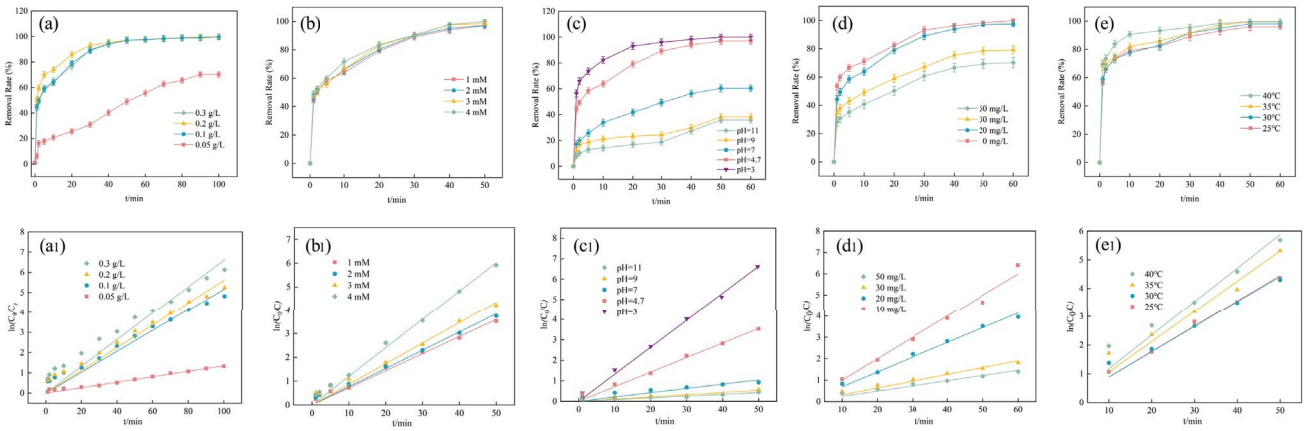

Fig. 4. Effect of reaction parameters on RhB removal at different experimental conditions (a–f) and pseudo-first-order reaction kinetics (a1–e1).

the activator dosage was elevated from 0.1 to 0.3 g/L after 100 min of reaction. Therefore, the active site on Fe-BC was not fully utilized. Furthermore, the Fe^{3+} leached from the reaction system with increased activator dosage, causing secondary pollution. Thus, the optimum experimental activator dosage was 0.1 g/L.

3.3.2. Effect of PS dosage on RhB removal

The PS dosage optimization counted as oxidant dosage is the primary factor associated with the cost of any AOPs. The RhB removal rate increased from 0.07192 mg/(L·min) (R^2 = 0.98341) to 0.12025 mg/(L·min) (R^2 = 0.99068) since the PS dosage was increased from 1 to 4 mM in Fig. 4b. In contrast, the RhB removal effect did not significantly enhance. The activation sites provided by Fe-BC are fixed. Thus, increasing PS concentration could improve the activation site efficiency. SO_4^{2-} reformed $S_2O_8^{2-}$ when an excessive quantity of PS was added. Then, SO_4^{2-} also reacted with persulfate to produce $S_2O_8^{2-}$, thus reducing PS utilization, as shown in Eqs. (2) and (3) [25,26]. Hydroxyl radical ($^{\bullet}OH$) was catalyzed by Fe-BC in PS solution, activating PS to SO_4^{2-} and improving the PS utilization efficiency [27]. Excess SO_4^{2-} could form stable sulfate with metals, which was corrosive and negatively affected the smell and taste of water. Overall, a PS dosage of 1 mM was considered due to experimental cost.

$$SO_4^{\bullet-} + SO_4^{\bullet-} \rightarrow S_2O_8^{2-} \quad (2)$$

$$SO_4^{\bullet-} + S_2O_8^{2-} \rightarrow SO_4^{2-} + S_2O_8^{\bullet-} \quad (3)$$

3.3.3. Effect of pH on RhB removal

As shown in Fig. 4c, the RhB removal rate by Fe-BC/PS decreased significantly with increasing pH, and the reaction rate constantly decreased from 0.13194 to 0.00845 mg/(L·min). The highest RhB removal efficiency was 99.96% at an initial solution pH of 3 after 60 min of a reaction than neutral (pH 7) and alkaline (pH 9 and 11) conditions. A similar dye degradation trend was investigated in the Fe catalyst-activated PS system [28], indicating that pH played a prominent role in $S_2O_8^{2-}$ oxidation and degradation. House [29] observed that HSO_4^- and H_2O_2 were produced from $S_2O_8^{2-}$ hydrolysis reactions, as represented in Eqs. (4) and (5). Su et al. [30] identified that pollutant removal was significantly inhibited when the pH was increased to 11 in the Fe_3O_4 activated PS system. This was associated with the protonation reaction occurring in acidic conditions, making the positively charged molecules susceptible to react with $SO_4^{\bullet-}$ than to the alkaline state. The acid-catalyzed effect of $S_2O_8^{2-}$ enhanced $SO_4^{\bullet-}$ production at low pH [31], thus increasing RhB removal. Low pH leads to Fe^{2+} dissolution, which could rapidly activate PS to synthesize reactive radicals for RhB removal [32]. Hydroxyl radicals became the primary reactive radical due to the gradual pH rise, and alkaline conditions cause H_2O_2 decomposition, as shown in Eq. (6). The HO_2^- produced after hydrolysis could react with $^{\bullet}OH$, depicted in Eqs. (7) and (8). HO_2^- could also react with the remaining H_2O_2 as in Eq. (9). HO_2^- reacting rate with $^{\bullet}OH$ was faster than reacting with H_2O_2. Moreover, the HO_2^- reaction showed a striking effect on $^{\bullet}OH$ removal. This lowered the rate of RhB removal using the Fe-BC/PS system. The optimal pH of 3 was selected for the follow-up experiments.

$$S_2O_8^{2-} + H_2O \rightarrow HSO_4^- + 0.5O_2 \quad (4)$$

$$S_2O_8^{2-} + 2H_2O \rightarrow 2HSO_4^- + H_2O_2 \quad (5)$$

$$H_2O_2 \rightarrow H^+ + HO_2^- \quad (6)$$

$$HO_2^- + {}^{\bullet}OH \rightarrow H_2O + O_2^- \quad (7)$$

$$HO_2^- + {}^{\bullet}OH \rightarrow {}^{\bullet}HO_2 + OH^- \quad (8)$$

$$H_2O_2 + HO_2^- \rightarrow H_2O + O_2 + {}^{\bullet}OH \quad (9)$$

3.3.4. Effect of initial dye concentration on RhB removal

As shown in Fig. 4d, the initial dye concentration significantly affected RhB removal. For example, the initial dye

concentration of RhB was 10 and 50 mg/L, and the removal rate was 99.96% and 70.2%, respectively, after 60 min of reaction, while other input variables were unchanged. Moreover, increasing dye concentration decreased the removal rate from 0.09985 to 0.02438 mg/(L·min). The reduction in removal efficiency and rate indicated that the Fe-BC/PS system could not produce enough active material to remove RhB at a higher dye concentration within a fixed activator and oxidant dosage [33]. Additionally, the intermediate products synthesized from the reaction competed with RhB to participate in the reaction as free radicals due to the increase in the initial dye concentration of RhB, causing a decline in the efficiency of RhB removal [33].

3.3.5. Effect of temperature on RhB removal

The RhB removal efficiency was increased with faster removal rate when the temperature increased, as shown in Fig. 4e. Thus, the increase in temperature could have accelerated the generation and reaction rate of •OH based on previous studies. Furthermore, PS could be thermally activated to produce $SO_4^{\bullet-}$, creating a difference in removing RhB [34]. In the Fe-BC/PS system, Fe-BC temperature increase and activation effect on PS have a superimposed impact on RhB removal, thereby elevating the removal rate. The optimal reaction temperature for environmental protection and energy saving was considered as 25°C.

3.3.6. Pseudo-first-order kinetic analysis

The experimental data were fitted well by pseudo-first-order kinetic as Eq. (10) follows. The fitting results are shown in Fig. 4a1–e1.

$$\text{The pseudo-first-order kinetic model: } \ln\frac{C_t}{C_0} = -kt \tag{10}$$

where t is the reaction time, C_0 is the initial concentration of RhB, and C_t is the concentration of RhB at the time of t, k is the rate constant of the pseudo-first-order kinetic model.

The reaction rate of RhB degradation (0.13194 min^{-1}) under optimum experimental conditions was approximate to that of RhB (0.1207 min^{-1}) under Mn^{2+}/Fe^{2+} homogeneous photocatalysis system, much faster than the degradation rate of NOR (0.0117 min^{-1}) with Fe_3O_4 activating PS [7,30].

3.3.7. Fe-BC stability experiments

Recycling experiments helped evaluate the reuse capacity of Fe-BC to decipher the practical applications of removing RhB. Fig. 3b indicates the results after four times use under optimum experimental conditions. The RhB removal rate was 45.6% in the second use under Fe-BC/PS system, showing good Fe-BC stability and reusability. The RhB removal rate was 25.39% in the third use compared to the first. Combining with the SEM in Fig. 1e, peanut shells were partially destroyed. The decrease in RhB removal could be associated with the change in the surface chemical structure of Fe-BC, catalytic site consumption, and the intermediate coverage of the RhB decomposition process [33,35]. Zhang et al. prepared Fe-SDBC to activate PS for the degradation of orange G; the removal rate was 23.07% in the third reuse. The reusability performance of Fe-BC in our study was similar to that of Fe-SDBC [33]. Moreover, the follow-up study could improve the Fe-BC recyclability performance.

3.4. Exploration of the catalytic mechanism

Fig. 5 shows the FTIR spectra of the BC, Fe-BC, and Fe-BC after the reaction. The absorption peak at 3,421 cm^{-1} could attribute to the stretching vibration of the C=O bond [36]. Moreover, the sharp peak at 1,075 cm^{-1} could correspond to the C–OH vibration in the carboxyl group [37]. The functional groups were detected in the FTIR spectra of the three materials (BC, Fe-BC, and Fe-BC after the reaction). The peak at 590 cm^{-1} corresponded to Fe_3O_4 [38], and 470 cm^{-1} was the Fe–O stretching vibration in α-Fe_2O_3 [38,39]. Both the functional groups were observed only in Fe-BC and Fe-BC post-reaction. After RhB absorption, some changes in the absorbent spectra were observed. The C=O peak vibration was shifted from 3,421 cm^{-1} (BC) to 3,324 cm^{-1} (Fe-BC), and the C–OH peak vibration in the carboxyl group was shifted from 1,075 cm^{-1} (BC) to 986 cm^{-1} (Fe-BC). These decreases and shifts in FTIR between BC and Fe-BC could be associated with the Fe–O–C chemical bonds formed between iron compounds and biochar [40]. The above analysis and SEM micrographs confirmed the successful modification of the material. As seen in Fig. 1d and e, some Fe-BC micropores were destroyed after the reaction compared to Fe-BC. Moreover, some pores were blocked, with agglomeration occurring between biochar, which could attribute to some intermediate products covering the Fe-BC surface. The Fe_3O_4 vibration peak of Fe-BC decreased after the reaction, with the Fe–O vibration peak disappearance. This proves that Fe-BC participated in the redox reaction, showing an activating effect on PS. The absorption peak at 1,588 cm^{-1} was attributed to C=C the stretching vibration [41], and at 1,021 cm^{-1} might be due to the C–H bond bending vibration of aromatic substances [42]. Both functional groups were only observed in Fe-BC after the reaction, probably due to the intermediate by-products attaching to the Fe-BC surface. Based on the functional groups, the reaction by-products

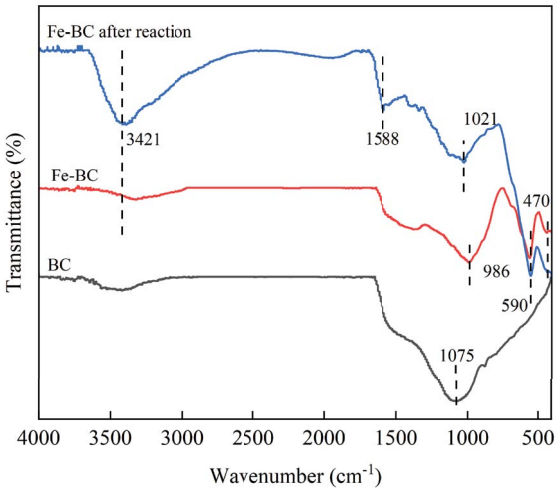

Fig. 5. FTIR spectra of BC, Fe-BC and Fe-BC after reaction.

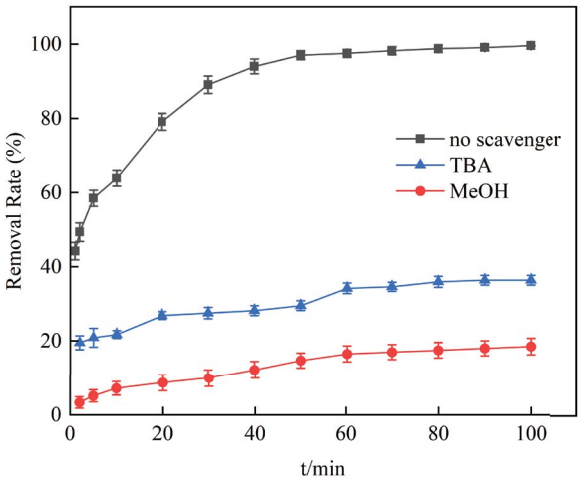

Fig. 6. Effect of quencher on RhB removal in Fe-BC/PS system.

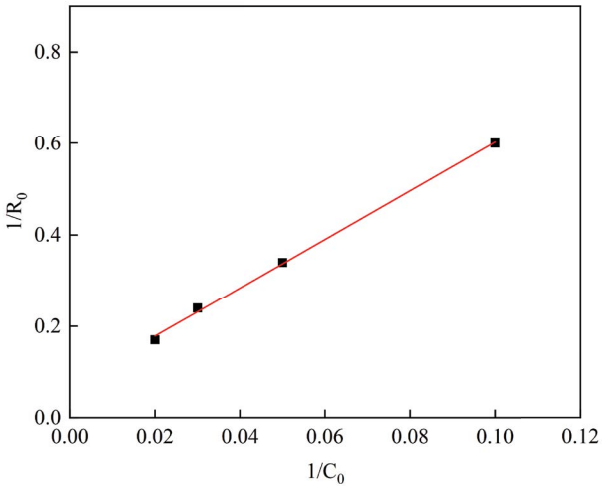

Fig. 7. L-H model of different initial RhB concentration.

could be aromatic unsaturated hydrocarbon organics. Generally, the more conductive sample part could transmit more electrons, providing a brighter image [43]. Hence, the regular-shaped bright white light could be inorganic matter containing Fe. This was involved in the reaction since the bright white light in Fig. 1f was significantly fainter than in Fig. 1g.

3.4.1. Free radical quenching experiments

Adding alcohols exerted a particular disincentive effect on RhB removal using the Fe-BC/PS system. In contrast, different alcohol quenchers could affect removing pollutants differently [43]. As shown in Fig. 6, the disincentive effects of methanol (MA) and tert-Butanol (TBA) addition on RhB removal by the Fe-BC/PS system were significant. Moreover, the RhB removal efficiency decreased to 18.52% and 36.43% after adding MA and TBA for 100 min, respectively. Thus, Fe-BC activation of PS in the Fe-BC/PS system synthesized $SO_4^{\bullet-}$ and $^{\bullet}OH$. Both the synthesized radicals played a significant role in the oxidative removal of RhB, with dominated $^{\bullet}OH$ [44].

3.4.2. Langmuir–Hinshelwood kinetic model fitting

Fig. 4d shows the Fe-BC/PS removal data of RhB at different initial dye concentrations. The data were used and linearly fitted based on the L-H model, as depicted in Fig. 7 and Eq. (10). The correlation coefficient R^2 = 0.99853 of the fitted equation indicated that the L-H model could accurately describe the RhB removal reaction process under Fe-BC/PS system as a synergistic effect of adsorption and reduction reaction. We obtained the reaction rate constant K_1 = 13.6937 mg/(L·min) and the adsorption rate constant K_2 = 0.01381 L/mg for Fe-BC/PS with RhB. K_1 was much larger than K_2, meaning that the reduction degradation of RhB was dominant and the adsorption rate controlled the reduction reaction rate [45]. The RhB reaction rate in this study was much faster than the degradation rate of trimethoprim with N-doped mulberry biochar activating PS and that of methylene blue with photocatalysis and hematite/biochar adsorption under the L-H kinetic model [46,47]. Additionally, the RhB adsorption rate was faster than the heterogeneous photocatalytic phenolic degradation rate reported by Asenjo et al. [48].

$$\frac{1}{R_0} = \frac{1}{K_1 K_2 C_0} + \frac{1}{K_1} \tag{11}$$

where R_0 represents the average reaction rate, mg/(L·min), K_1 is the reaction rate constant, mg/(L·min), and K_2 is the Langmuir adsorption constant, L/mg.

4. Conclusion

Fe-BC is a novel biological material and a promising method in dying wastewater treatment to activate PS and remove RhB. The Fe-BC activity was successfully verified after modification. The optimum reaction condition was obtained at 25°C, the Fe-BC dosage was 0.1 g/L, the PS dosage was 1 mM, the initial RhB concentration was 20 mg/L, and pH was 3 in the Fe-BC/PS system, and the maximum removal was achieved (99.96%). The RhB absorption rate is followed by a pseudo-first-order reaction. The Langmuir–Hinshelwood model was well fitted to the data of different initial RhB concentrations, indicating that RhB removal is a synergistic effect of adsorption and degradation. Free radical quenching experiments revealed that Fe-BC could remove RhB by activating persulfate to produce $SO_4^{\bullet-}$ and $^{\bullet}OH$, with a significant role of $^{\bullet}OH$ in the reaction process. Therefore, Fe-BC/PS based on AOPs can effectively treat dying wastewater.

Funding

This research was funded by Shandong Provincial Natural Science Foundation (ZR2020MD108), Program of Zibo school city fusion (2021JSCG0012).

Declarations

The authors report there are no competing interests to declare.

CRediT authorship contribution statement Yang Yang: Conceptualization, Methodology, Writing-original draft, Visualization. Hongyang Lin: Validation, Writing-review & editing. Shuhui Wu: Investigation, Data curation. Xue Yao: Investigation, Formal analysis. Xuedong Feng: Writing-review & editing, Supervision, Funding acquisition. Yanfei Ma: Writing-review & editing, Project administration, Funding acquisition.

References

[1] D.M. Ren, Q.X. Yu, Y. Zhao, Q.W. Ai, Y.L. Wu, Y. Zhao, Research progress of physical method for removing Rhodamine B from wastewater, J. Bohai Univ., Nat. Sci. Ed., 41 (2020) 97–104.

[2] L. Zhong, J.J. Chen, Technical progress in organic effluent water treatment by advanced oxidation processes, Ind. Water Treat. (TianJin, China), 1 (2002) 1–5.

[3] Z.J. Guan, H.Y. Huang, Progress in the degradation of organic matter by activated persulfate from polymetallic iron oxides, Appl. Chem. Ind. (Xi'an, China), 50 (2021) 1049–1055.

[4] R. Yang, The Study of Rhodamine B Degradation by Fenton and Activated Persulfate Process, Xi'an University of Architecture and Technology, 2015.

[5] Z.P. Yang, X.T. Lv, X.Q. Liu, S.M. Jia, Y.Y. Zhang, Y.Y. Yu, C.J. Zhang, D.D. Liu, Sieve-like CNT film coupled with TiO_2 nanowire for high-performance continuous-flow photodegradation of Rhodamine B under visible light irradiation, Nanomaterials, 11 (2021) 1335, doi: 10.3390/nano11051335.

[6] Y.P. Cui, Z.W. Zhou, Y. Gao, L.D. Lei, J.G. Cao, R.J. Wu, L.L. Liang, Z.Q. Huang, Energy saving intermittent electro-Fenton system combined with commercial MoS_2 for effective Rhodamine B degradation, J. Cleaner Prod., 289 (2021) 125807, doi: 10.1016/j.jclepro.2021.125807.

[7] Y. Liang, H.T. Ren, J. Han, H. Li, J.W. Liu, Study on the photodegradation of Rhodamine B by Mn^{2+}/Fe^{2+} and SO_3^{2-}/Fe^{2+} homogeneous systems, New Chem. Mater., 48 (2020) 209–213.

[8] H.Z. Wang, W.Q. Guo, N.Q. Ren, Development and application of biochar-based metal-free persulfate activators, Acta Sci. Circum., 40 (2020) 3582–3589.

[9] A.H. Cheng, W.C. Ma, Z. Xu, Treatment of phenol wastewater with persulfate activated by plasma-modified sponge iron, Chem. Ind. Eng. Prog., 39 (2020) 798–804.

[10] H.D. Xu, Y.C. Zhang, J.J. Li, Q.Q. Hao, X. Li, F.H. Liu, Heterogeneous activation of peroxymonosulfate by a biochar-supported Co_3O_4 composite for efficient degradation of chloramphenicols, Environ. Pollut., 257 (2020) 113610, doi: 10.1016/j.envpol.2019.113610.

[11] J.L. Ding, W.H. Xu, S.B. Liu, Y.G. Liu, X.F. Tan, X. Li, Z.W. Li, P. Zhang, L. Du, M.F. Li, Activation of persulfate by nanoscale zero-valent iron loaded porous graphitized biochar for the removal of 17β-estradiol: synthesis, performance and mechanism, J. Colloid Interface Sci., 588 (2021) 776–786.

[12] H. Qu, L. Chen, F.J. Yang, J.W. Zhu, C.D. Qi, G.L. Peng, Synthesis of an environmentally friendly modified mulberry branch-derived biochar composite: high degradation efficiency of BPA and mitigation of toxicity in silkworm larvae, Int. J. Mol. Sci., 24 (2023) 3609, doi: 10.3390/ijms24043609.

[13] S.F. Jiang, L.L. Ling, W.J. Chen, W.J. Liu, D.C. Li, H. Jiang, High efficient removal of Bisphenol A in a peroxymonosulfate/iron functionalized biochar system: mechanistic elucidation and quantification of the contributors, Chem. Eng. J., 359 (2019) 572–583.

[14] H.C. Fu, P. Zhao, S.J. Xu, G. Cheng, Z.Q. Li, Y. Li, K. Li, S.L. Ma, Fabrication of Fe_3O_4 and graphitized porous biochar composites for activating peroxymonosulfate to degrade p-hydroxybenzoic acid: insights on the mechanism, Chem. Eng. J., 375 (2019) 121980, doi: 10.1016/j.cej.2019.121980.

[15] F.L. Shao, Y.J. Wang, Y.R. Mao, T. Shao, J.G. Shang, Degradation of tetracycline in water by biochar supported nanosized iron activated persulfate, Chemosphere, 261 (2020) 127844, doi: 10.1016/j.chemosphere.2020.127844.

[16] H.H. Lyu, B. Gao, F. He, A.R. Zimmerman, C. Ding, J.C. Tang, J.C. Crittenden, Experimental and modeling investigations of ball-milled biochar for the removal of aqueous methylene blue, Chem. Eng. J., 335 (2018) 110–119.

[17] H.R. Hao, Q. Zhang, Y. Qiu, L. Meng, X.N. Wei, W.J. Sang, J.W. Tao, Insight into the degradation of Orange G by persulfate activated with biochar modified by iron and manganese oxides: synergism between Fe and Mn, J. Water Process Eng., 37 (2020) 101470, doi: 10.1016/j.jwpe.2020.101470.

[18] J. Xu, X.L. Zhang, C. Sun, H. He, Y.X. Dai, S.G. Yang, Y.S. Lin, X.H. Zhan, Q. Li, Y. Zhou, Catalytic degradation of diatrizoate by persulfate activation with peanut shell biochar-supported nano zero-valent iron in aqueous solution, Int. J. Environ. Res. Public Health, 15 (2018) 1937, doi: 10.3390/ijerph15091937.

[19] A. Ikhlaq, H.Z. Anwar, F. Javed, S. Gull, Degradation of safranin by heterogeneous Fenton processes using peanut shell ash-based catalyst, Water Sci. Technol., 79 (2019) 1367–1375.

[20] Q. An, C.L. Liu, S.M. Deng, Y.X. Jiao, M. Tang, M.L. Yang, Z.H. Ye, B. Zhao, Resource utilization of agricultural waste: converting peanut shell into an efficient catalyst in persulfate activation for degradation of organic pollutant, Chemosphere, 304 (2022) 135308, doi: 10.1016/j.chemosphere.2022.135308.

[21] L. Shi, L. Liang, J. Ma, F.X. Wang, J.M. Sun, Remarkably enhanced photocatalytic activity of ordered mesoporous carbon/g-C_3N_4 composite photocatalysts under visible light, Dalton Trans., 43 (2014) 7236–7244.

[22] M. Muttakin, S. Mitra, K. Thu, K. Ito, B.B. Saha, Theoretical framework to evaluate minimum desorption temperature for IUPAC classified adsorption isotherms, Int. J. Heat Mass Transfer, 122 (2018) 795–805.

[23] J. Wang, Study on Treatment of Refractory Organic Wastewater by Persulfate Activated by Iron Based Sludge-derived Biochar, Huazhong University of Science and Technology, 2017.

[24] C.J. Liang, Y.Y. Guo, Mass transfer and chemical oxidation of naphthalene particles with zerovalent iron activated persulfate, Environ. Sci. Technol., 44 (2010) 8203–8208.

[25] D.O. Yang, J.C. Yan, L.B. Qian, Y. Chen, L. Han, A.Q. Su, W.Y. Zhang, H. Ni, M.F. Chen, Degradation of 1,4-dioxane by biochar supported nano magnetite particles activating persulfate, Chemosphere, 184 (2017) 609–617.

[26] Z.Y. Dong, Q. Zhang, B.Y. Chen, J.M. Hong, Oxidation of Bisphenol A by persulfate via Fe_3O_4-α-MnO_2 nanoflower-like catalyst: mechanism and efficiency, Chem. Eng. J., 357 (2019) 337–347.

[27] J.G. Kim, S.M. Park, M.E. Lee, E.E. Kwon, K. Baek, Photocatalytic co-oxidation of As(III) and Orange G using urea-derived g-C_3N_4 and persulfate, Chemosphere, 212 (2018) 193–199.

[28] C. Cai, L.G. Wang, H. Gao, L.W. Hou, H. Zhang, Ultrasound enhanced heterogeneous activation of peroxydisulfate by bimetallic Fe-Co/GAC catalyst for the degradation of Acid Orange 7 in water, J. Environ. Sci. (China), 26 (2014) 1267–1273.

[29] D.A. House, Kinetics and mechanism of oxidations by peroxydisulfate, Chem. Rev., 62 (1961) 185–203.

[30] B.Q. Su, Y.Q. Liu, Y.T. Lin, J. Wang, X.H. Quan, R. Li, C.X. Rui, Simultaneous removal of norfloxacin and Pb(II) via Fe_3O_4-activated persulfate oxidation, China Environ. Sci., 42 (2022) 717–727.

[31] T. Taghipour, G.R. Karimipour, M. Ghaedi, M.R. Rahimi, S. Mosleh, Sonophotocatalytic treatment of diazinon using visible light-driven Ce:Cu-1,4-BDOAH$_2$ photocatalyst in a batch-mode process: response surface methodology and optimization, Appl. Organomet. Chem., 32 (2018) e3962, doi: 10.1002/aoc.3962.

[32] S.H. Do, Y.J. Kwon, S.H. Kong, Effect of metal oxides on the reactivity of persulfate/Fe(II) in the remediation of diesel-contaminated soil and sand, J. Hazard. Mater., 182 (2010) 933–936.

[33] Q. Zhang, C.F.Y. Xie, Y. Qiu, M. Li, Z.X. Fan, L.Q. Wang, Durable degradation of orange G using persulfate activated by sludge-derived heterogeneous catalyst, China Environ. Sci., 39 (2019) 3879–3886.

[34] X.G. Gu, S. Lv, Z.X. Qiu, Q. Sui, K. Lin, Y. Liu, Oxidation of 1,1,1-trichloroethane in aqueous and slurry systems by

thermally activated persulfate, Acta Sci. Circum., 32 (2012) 1374–1380.
[35] J. Leichtweis, S. Silvestri, E. Carissimi, New composite of pecan nutshells biochar-ZnO for sequential removal of Acid red 97 by adsorption and photocatalysis, Biomass Bioenergy, 140 (2020) 105648, doi: 10.1016/j.biombioe.2020.105648.
[36] H. Jaberi, S. Mosleh, K. Dashtian, Development of cigarette carbonaceous hydrochar/ZIF-67-based fluids for CO_2 capture from a gas stream in a packed column: mass-transfer performance evaluation, Energy Fuels, 34 (2020) 7295–7306.
[37] B. Jafari, M.R. Rahimi, M. Gheadi, K. Dashtian, S. Mosleh, CO_2 capture by amine-based aqueous solution containing atorvastatin functionalized mesocellular silica foam in a counter-current rotating packed bed: central composite design modeling, Chem. Eng. Res. Des., 129 (2018) 64–74.
[38] A. Puri, D. Dev, D.N. Prasad, S. Hira, R. Sharma, Modified okra gum with silica: a novel superdisintegrant for fast disintegrating tablet, J. Drug Deliv. Therapeutics, 9 (2019) 206–211.
[39] T. Chen, Z.Y. Zhou, S. Xu, H.T. Wang, W.J. Lu, Adsorption behavior comparison of trivalent and hexavalent chromium on biochar derived from municipal sludge, Bioresour. Technol., 190 (2015) 388–394.
[40] J.C. Yan, L. Han, W.G. Gao, X. Song, M.F. Chen, Biochar supported nanoscale zerovalent iron composite used as persulfate activator for removing trichloroethylene, Bioresour. Technol., 175 (2015) 269–274.
[41] P. Devi, A.K. Saroha, Simultaneous adsorption and dechlorination of pentachlorphenol from effluent by Ni-ZVI magnetic biochar composites synthesized from paper mill sludge, Chem. Eng. J., 27 (2015) 195–203.
[42] L. Qin, Z.W. Li, Z.H. Xu, X.W. Guo, G.L. Zhang, Organic-acid-directed assembly of iron–carbon oxides nanoparticles on coordinatively unsaturated metal sites of MIL-101 for green photochemical oxidation, Appl. Catal., B, 172 (2015) 500–508.
[43] M.N. Ahsan, P.R.P. Verma, Enhancement of in vitro dissolution and pharmacodynamic potential of olanzapine using solid SNEDDS, J. Pharm. Invest., 48 (2018) 269–278.
[44] X.D. Zha, Z.W. Wang, A.H. Liu, G.Y. Qian, Experimental Experimental Analysis on Material Properties for Buton Rock Asphalt and Its Modified Asphalt, Transportation Research Congress, Beijing , China, 2017, pp. 23–25.
[45] Z.H. Xie, Study on Remove of 2,4,6-TCP by Nano Fe/Ni Loaded by Crofton Weed Biochar Jointly with $K_2S_2O_8$, Chengdu University of Technology, 2019.
[46] S. Annamalai, W.S. Shin, Efficient degradation of trimethoprim with ball-milled nitrogen-doped biochar catalyst via persulfate activation, Chem. Eng. J., 440 (2022) 135815, doi: 10.1016/j.cej.2022.135815.
[47] M.F. Arkaan, R.F. Ekaputri, I. Fatimah, A. Kamari, Physico-chemical and photocatalytic activity of hematite/biochar nanocomposite prepared from *Salacca* skin waste, Sustainable Chem. Pharm., 16 (2020) 100261, doi: 10.1016/j.scp.2020.100261.
[48] N.G. Asenjo, R. Santamaría, C. Blanco, M. Granda, P. Álvarez, R. Menéndez, Correct use of the Langmuir–Hinshelwood equation for proving the absence of a synergy effect in the photocatalytic degradation of phenol on a suspended mixture of titania and activated carbon, Carbon, 55 (2013) 62–69.